CHEMISTRY OF MATERIALS
Cite This: Chem. Mater. 2019, 31, 8927−8936
Article
pubs.acs.org/cm

# Photo-Oxidation Reveals H-Aggregates Hidden in Spin-Cast-Conjugated Polymer Films as Observed by Two-Dimensional Polarization Imaging

Juanzi Shi,[†] Xiaofeng Xu,[‡] Yuxin Xia,[§] Ruiyun Chen,[∥] Zafer Hawash,[⊥] Dargie Deribew,[⊥] Ellen Moons,[⊥] Olle Inganäs,[§] and Ivan G. Scheblykin*[,†]

[†]Chemical Physics and NanoLund, Lund University, P.O. Box 124, SE-22100 Lund, Sweden
[‡]Department of Materials Science and Engineering, Ocean University of China, Qingdao 266100, China
[§]Department of Physics, Chemistry and Biology (IFM), Linköping University, S-581 83 Linköping, Sweden
[∥]Institute of Laser Spectroscopy, Shanxi University, Taiyuan 030006, China
[⊥]Department of Physics, Karlstad University, SE-65188 Karlstad, Sweden

Supporting Information

**ABSTRACT:** Spin-cast intermolecular interactions in conjugated polymer films lead to the formation of excited states delocalized over a few oriented and tightly packed conjugated segments. The optoelectronic properties of conjugated polymers are strongly dependent on the presence of such oriented domains at a nanoscale level. We observe oriented domains as large as several micrometers in size spontaneously formed in spin-cast PBDT-TPD films. Two-dimensional polarization imaging of fresh and photodegraded films showed a much higher visibility of the oriented domains in the degraded samples. We propose that the film is a mixture of two phases with different degrees of chain alignment. The photoluminescence of the more anisotropic phase is more stable against photodegradation in comparison with the less anisotropic phase. Photodegradation predominately quenches photoluminescence of the less anisotropic phase making the oriented domains more visible in the polarization contrasts. Spectral and energy transfer properties of the more oriented phase allowed us to assign it to weakly coupled H-aggregates with the suppressed 0−0 vibronic transition. Stable photoluminescence of H-aggregates in comparison with that of nonaggregated (less oriented) chains may help to understand degradation mechanisms of polymer devices and shows the role of energy transfer in this process. Selective degradation-induced quenching can reveal hidden inhomogeneity of conjugated polymer films.

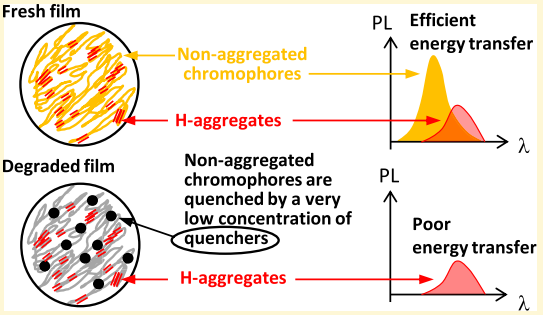


## INTRODUCTION

Conjugated polymers (CPs) possess optical and electronic properties of semiconductors. This makes them highly interesting from the point of view of fundamental photophysics and physical chemistry as well as for technology, where organic field-effect transistors,[1] organic light emitting diodes,[2] photovoltaic cells,[3] electrochemical transistors for bioelectronics and sensors,[4−6] and devices for neuromorphic computing[7] are just a few applications to mention.

CPs possess $\pi$-conjugated systems, extended along the chain backbone, making a clear correlation between the chain direction and the direction of the optical transition dipole moments. An isolated chain can be seen, at the first approximation, as a set of segments (chromophores), where the direction of the transition dipole moment coincides with the direction of the backbone of the segment.

CP chains in a film can adopt different conformations; however, contrary to insulating polymers where only mechanical properties are influenced, here the chain organization becomes also extremely important for the optical and electronic properties of the materials. This is because of the electronic interactions between the closely situated chain segments. Dense chain packing can be reached only when polymers chains arrange, at least locally, in a quasi-parallel fashion, creating conditions for the formation of collective excitons and partially charge separated excitations.

Indeed, due to the strong transition dipole moments and the close distance between the chain segments, exciton coupling between chromophores must be considered. Exciton coupling leads to delocalization of the excitation over two or more segments and can be J-type for head to tail arrangement, or H-type for parallel arrangement of dipoles. Weak J-coupling leads to a slight red shift of the spectra and, in principle, has a similar effect as increasing of the effective conjugation length.

Received: July 27, 2019
Revised: October 18, 2019
Published: October 19, 2019






DOI: 10.1021/acs.chemmater.9b02996
Chem. Mater. 2019, 31, 8927−8936

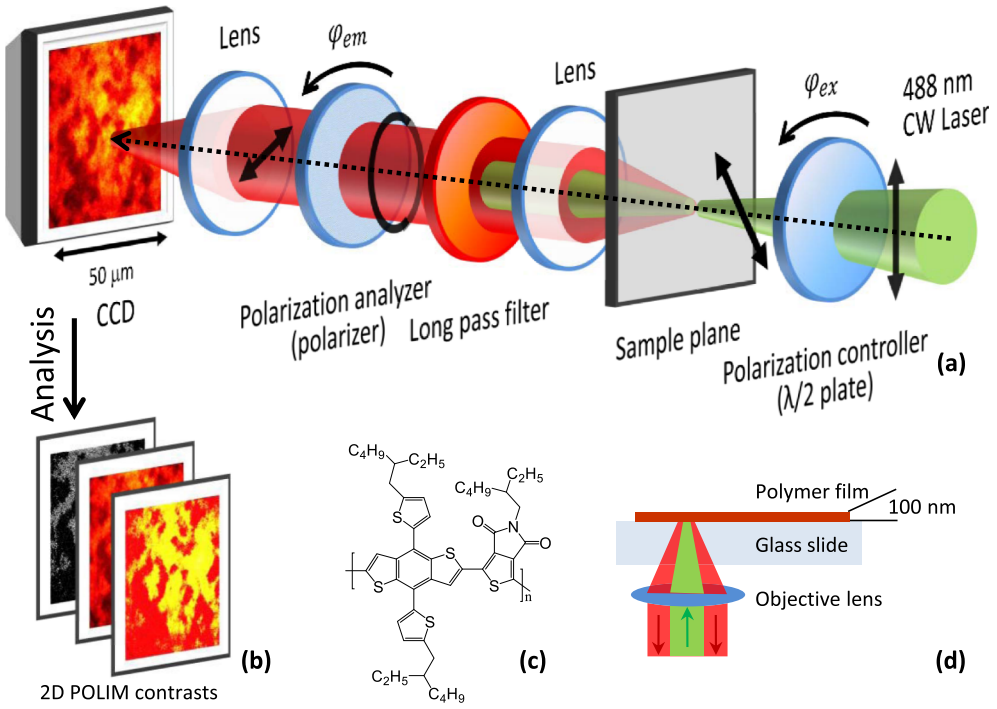


**Figure 1.** (a) Principle scheme of the 2D POLIM experiment. The sample is excited using linearly polarized light with the electric field vector oriented at an excitation angle $\varphi_{ex}$. Another polarizer (analyzer with a transmission angle $\varphi_{em}$) placed in the emission path is used to probe the polarization properties of luminescence. The luminescence images are recorded at different combinations of the excitation angle $\varphi_{ex}$ and emission probe angles $\varphi_{em}$ by an EMCCD camera. (b) 2D POLIM contrasts such as modulation depths and phases of excitation and emission, are obtained by analyzing the luminescence intensity in each pixel of the image as a function of $\varphi_{ex}$ and $\varphi_{em}$. (c) Chemical structure of the polymer PBDT-TPD. (d) Illustration of the epifluorescence experimental geometry used in this work (laser—green, luminescence—red); the film thickness was about 100 nm.

However, weak H-coupling, besides slight blue-shifting of the spectra, suppresses 0−0 vibronic transitions relative to 0−1 and other vibronic transitions.[8] This leads to drastic changes in the absorption and luminescence spectra. In a real polymer film J- and H-coupling exist probably at the same time, in different local regions, leading to substantial inhomogeneous broadening of the spectra and also affecting the fluorescence lifetime and photoluminescence (PL) quantum yield in a complicated and not fully rationalized manner.[9,10]

Spin-cast films of CPs without any noticeable optical anisotropy within the plane of the film ($x$−$y$ plane) can be formed, but often the optical characteristics (like, e.g., refractive index) are different for light with the electric field direction normal ($z$-direction) versus parallel ($x$−$y$ plane) to the film plane.[11−17] This happens because $\pi$-conjugation is typically planar, so the chains look like ribbons and there is a preferential orientation of the conjugated planes relative to the substrate surface. Preferential orientation in the $x$−$y$ plane also can exist locally in the film; however, with optical resolution it is usually not visible because individual oriented domains are often too small compared to the resolution of the optical microscope and their orientation is random. The size of the oriented domains with distinct polarization in the $x$−$y$ plane varies from several to hundreds of nanometers, depending on the structure of the polymers and the film preparation process.[18−20] Single molecule spectroscopy studies directly showed highly oriented chain conformation possessing high polarization in absorption and emission.[21,22] However, ensemble averaging in films eliminates polarization anisotropy making films optically uniform.

The ability of polymer chains to orient in films is determined by their chemical structure. Some polymers indeed readily form polycrystalline films with micrometre or even larger domains.[23−27] One can see a semicrystalline film as a mixture of monocrystalline (crystal) and noncrystalline (amorphous) where small crystalline domains extend their order over a larger scale via a high degree of interconnectivity through tie-molecules. Note that long range order is a quite desirable property for obtaining high and anisotropic charge mobility.[25] Preferential orientation on scales of millimeters and larger can be induced for some CPs using external stimulus, including deposition on a liquid substrate,[28] mechanical rubbing,[29] epitaxial growth and unidirectional deposition techniques,[30] in situ photo-polymerization on nematic liquid crystals,[31] and other methods. The morphology of polycrystalline polymer films has been studied by scanning probe near-field optical microscopy,[27] polarized charge modulation spectroscopy,[25] transmission electron microscopy,[26] near edge X-ray absorption fine structure,[24] and scanning transmission X-ray microscopy.[23,24]

In this paper we report an observation of spontaneously formed highly oriented domains of several micrometers in films of the CP PBDT-TPD prepared by the standard spin-casting method. This studied polymer has not been known before to possess any polycrystalline properties at a large spatial scale. X-ray scattering has shown this polymer to be partially crystalline, albeit with small domains.[32] We studied these domain structures using polarization fluorescence microscopy and in particular two dimensional polarization imaging (2D POLIM). We found that the polymer film is a mixture of less oriented and more oriented phases where the latter show a red-shifted


DOI: 10.1021/acs.chemmater.9b02996
Chem. Mater. 2019, 31, 8927−8936

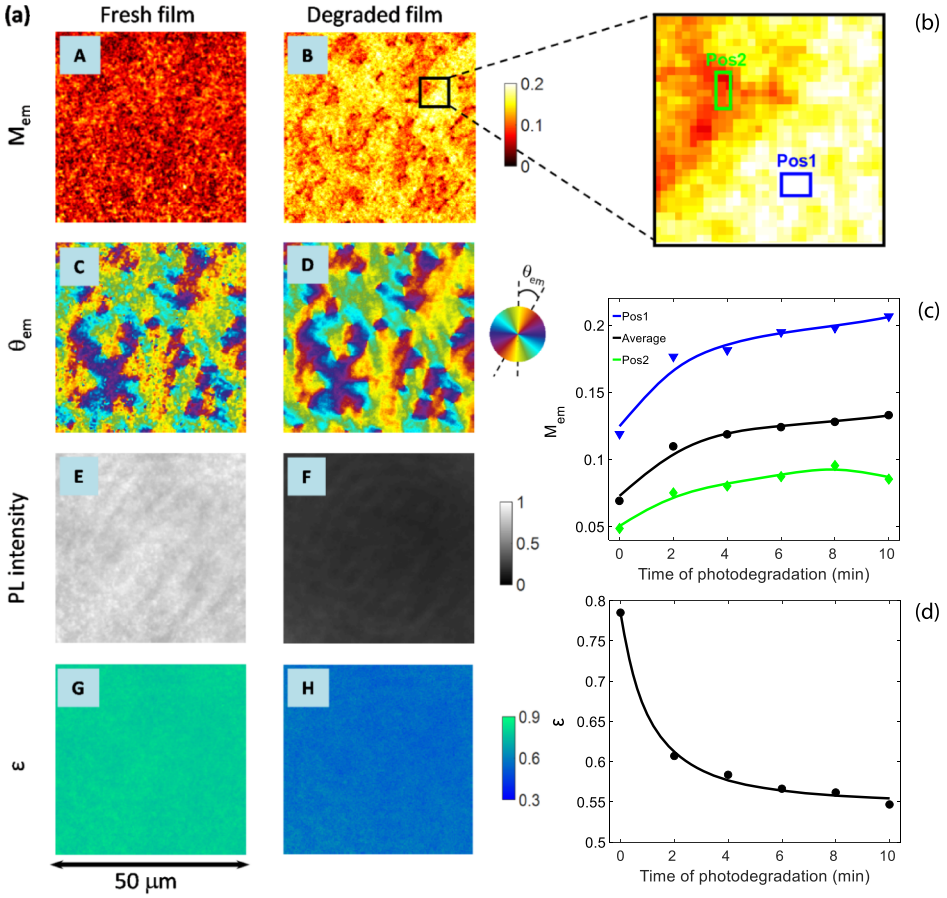


**Figure 2.** (a) Exemplary 2D POLIM images of the same position on the fresh (left column) and degraded (right column) PBDT-TPD film prepared on the glass substrate, spatial resolution is about 1 $\mu$m. The images in 2D POLIM contrasts are emission modulation depth $M_{em}$ (A,B), modulation phase of emission $\theta_{em}$ (C,D), fluorescence intensity (E,F), and energy transfer efficiency (G,H). The size of the six images is 50 $\mu$m × 50 $\mu$m. (b) Zoom-in of the area marked in image a(B). Two positions are marked in this region: Pos1 (blue rectangular, high $M_{em}$) and Pos2 (green rectangular, low $M_{em}$). (c) Evolution of $M_{em}$ averaged over the area of Pos1 (blue curve with triangle marks), Pos2 (green curve with diamond marks), and of the whole sample area shown in (a) (black curve with round marks) during the photodegradation. (d) Time evolution of $\varepsilon$ averaged over the whole area of the sample shown in (a) during photodegradation (black curve with round marks).

PL spectrum. The ratio between the two phases depends on the substrate and other preparation conditions. These two phases show different luminescence spectra and also a different stability against photo-oxidation. The last effect allowed us to use photo-oxidation as a tool to make (to "develop" in analogy to the photographic film processing) the pattern of the polarized domains visible, which is hardly visible in freshly prepared films. We assign the more oriented structures to weakly coupled H-aggregates which are always present in the film; however, their contribution to fluorescence is usually screened by the dominant luminescence from local emitting sites in the less oriented nonaggregated phase. We also found that long-range excitation energy transfer (EET), although very efficient within the nonaggregated phase, is much less efficient for excitons trapped in H-aggregates. We believe that the observed correlation between the structure, spectral properties, and photostability will be useful for further understanding the factors limiting the efficiency and stability of polymer photovoltaic devices.

## ■ MATERIALS AND METHODS

The $\pi$-CP poly[4,8-bis(5-(2-ethylhexyl)thiophen-2-yl)benzo[1,2-*b*:4,5-*b*′] dithiophene-2,6-diyl-*alt*-(5-(2-ethylhexyl)-4*H*-thieno[3,4-*c*]pyr-role-4,6(5*H*)-dione)-1,3-diyl] (PBDT-TPD, Figure 1c) is a known donor material for polymer solar cells.[32−38] The synthesis of PBDT-TPD with weight-average molecular weight $M_w$ = 83.8 kDa is described in details elsewhere.[32] To prepare the spin-cast films, the glass substrates were cleaned by 2% Hellmanex III solution at 35° in an ultrasonic bath for 30 min, then washed with Milli-Q water three times and exposed to ozone generated in a UV lamp chamber (254 nm) for 30 min. The PBDT-TPD polymer film was prepared by spin-casting at 990 rpm of 12.5 mg/mL solution of PBDT-TPD in chloroform on a clean glass substrate, which resulted in a film thickness of about 100 nm. For photodegradation, the films were exposed to circularly polarized light at 488 nm with a power density as high as 10 W/cm$^2$ over a 100 $\mu$ sized area for 10 minutes under ambient conditions. All the followed measurements (2D POLIM, PL spectra, absorption spectra and PL decay) were carried out under a nitrogen atmosphere (where the degradation process was much slower even at a high excitation power) and low excitation power density (0.01 W/cm$^2$) to avoid extra sample degradation.

Luminescence properties of the films were studied using two home-built wide-field epifluorescence microscopes based on Olympus IX71 equipped with 40× (NA = 0.6) dry objective lens; the geometry of the experiment is shown in Figure 1d. One of the microscopes was designed for polarization (2D POLIM) and spectral measurements and the other for luminescence kinetics measurements.

The principle of the two-dimensional polarization imaging (2D POLIM) technique is illustrated in Figure 1a. The sample was excited by a 488 nm CW Ar-ion laser and the PL image was acquired by an EMCCD (Princeton Instruments, Photonmax 512B) camera. One


DOI: 10.1021/acs.chemmater.9b02996
*Chem. Mater.* 2019, 31, 8927−8936

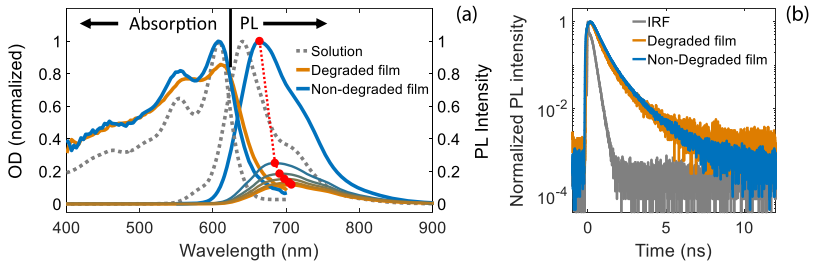


**Figure 3.** (a) The PL and absorption spectra of isolated chains in diluted chloroform solution (grey dashed line) in comparison to those of the spin-cast film on a glass substrate (solid thick lines, blue—nondegraded film, orange—after 10 min of degradation). Absorption and PL spectra of the solution are normalized. PL spectra of the film were recorded every 2 min during photodegradation. These spectra are plotted in units of the maximum PL intensity of the fresh film. The red dashed line shows the red shift of the PL spectral maximum. Absorption spectra of the film before and after degradation are plotted in units of the maximum optical density of the fresh film. (b) The PL decay kinetics measured from the same positions as the PL spectra showed in (a): solid blue line—before degradation, solid orange line—after degradation. The grey line is the instrument response function.

pixel of the camera corresponds to a square of 260 nm × 260 nm at the sample plane. The practical resolution of our imaging system was about 1 $\mu$m (4 pixels) in the 700 nm emission region. 24 luminescence images were acquired for different combinations of the angles $\varphi_{ex}$ and $\varphi_{em}$, so that we can obtain one full polarization portrait $I(\varphi_{ex}, \varphi_{em})$ for each pixel on the PL image, where $I$ is the PL intensity.

Polarization portraits are used to characterize the sample's internal chromophore geometry and the EET between chromophores.[28,39−41] In brief, the integrals of the polarization portrait over the excitation or emission angles have the functional form: $I_0[1 + M(\cos(2[\varphi - \theta]))]$, where $I_0$ is the averaged PL intensity and $M$ is either the modulation depths in excitation, $M_{ex}$ (2D plot integrated over $\varphi_{em}$) or emission, $M_{em}$ (2D plot integrated over $\varphi_{ex}$). The modulation depths are the widely used parameters to describe the degree of alignment of transition dipole moments.[42] They range from 0 to 1 for isotropic to fully oriented systems, respectively. The polarization phases in excitation ($\theta_{ex}$) and emission ($\theta_{em}$) represent the main orientation axes of the absorbing and emissive dipoles. It is worthy to mention that the definition of phases is meaningless if M is close to zero. In our experiments, we consider the value of phase to be reliable when $M >$ 0.06. The differences between $M_{ex}$ and $M_{em,}$ as well as between $\theta_{ex}$ and $\theta_{em}$, are the indications of EET. Furthermore, the analysis of the full polarization portrait based on single funnel approximation provides a unique parameter, called energy funnelling efficiency ($\varepsilon$),[43] This parameter quantifies the EET on the scale from 0 to 1, which corresponds to the situation ranging from independent chromophores (no EET), to the one of the complete energy funnelling to a single emitting site or an EET emitter. More about the energy funnelling efficiency parameter and its advantages over traditional fluorescence anisotropy can be found elsewhere.[42−44] The parameters $I_0$, $M_{ex}$, $M_{em}$, $\theta_{ex}$, $\theta_{em}$, and $\varepsilon$, measured in each pixel, give us images of the sample in the 2D POLIM contrasts as illustrated in Figure 1b. Because of the light diffraction limit, the spatial resolution of our imaging system is about 1 $\mu$m. Therefore, all the above parameters are actually averaged over a 1 × 1 $\mu m^2$ area and the thickness of the film (100−200 nm). More details about the data analysis of 2D POLIM measurement can be found in Section S1 of the Supporting Information.

The PL spectra were obtained for the same positions in the films investigated by 2D POLIM using the same excitation laser (488 nm). For that the required region of the sample was selected by a vertical slit placed in the first image plane. A transmission diffraction grating was placed before the camera chip to give the image of the sample region in the zero diffraction order and the corresponding spectrum in the first diffraction order. Local absorption spectra were calculated from transmission spectra measured in the same microscope setup described above, using a white light source (Olympus, U-LH100-3) instead of a laser, as described in more details elsewhere.[45] PL decay kinetics were measured using the 485 nm-pulsed diode laser operated at 20 MHz (PicoQuant GmbH, PDL 828), the time-correlated single-photon counting unit (PicoQuant GmbH, PicoHarp 300), and the avalanche photodiode (Micro Photon Devices, PDM series). The instrumental response function (Figure 3b) was 190 ps.

## RESULTS

We obtained a series of images with 2D POLIM contrasts of the very same region of the sample before and after photodegradation, shown in Figure 2a, left column, and Figure 2a, right column, respectively. Figures 2a and 3a show that the PL intensity decreases drastically upon illumination of the sample under ambient conditions by 10 W/cm$^2$ power density at 488 nm for 10 min, while the absorption of the film practically did not change.

The 2D POLIM was running every 2 min to obtain the data shown in Figure 2c,d, where the average values of the modulation depths and energy transfer efficiency ($\varepsilon$) are presented as a function of the degrading time. To avoid degradation during the 2D POLIM measurement, which lasted 1.5 min, the sample was temporarily placed in nitrogen atmosphere and the laser power was reduced to 0.01 W/cm$^2$.

The emission modulation depth, reflecting the degree of alignment of the transition dipole moments (averaged over the microscope spatial resolution), increased in average over the whole image shown in Figure 2 approximately two times upon photodegradation. However, $M_{em}$ increased to a different extent at different spatial locations (Figure 2b,c, compares Pos1 and Pos2) leading to a clear microscale pattern (spatial inhomogeneity) to appear in the $M_{em}$ image of the degraded film [Figure 2a(B)]. Note that there is no obvious change in phase images apart from becoming sharper and clearer [Figure 2a(C,D)], which means that the microstructure was present already in the fresh film and becomes just more visible after photodegradation. A similar effect can also be observed in the films of different thickness, of which the thickest film tested was around 200 nm.

In order to check if the induced degradation led to a change in the film structure, the film surface was imaged by atomic force microscopy (AFM) before and after degradation. The BDT unit (benzo[1,2-*b*:4,5-*b*′]dithiophene) of the polymer backbone has good $\pi-\pi$ stacking properties because of its large, rigid, and coplanar structure,[46] so, as expected, the freshly spin-cast PBDT-TPD film appears smooth and homogeneous with very little surface roughness as shown by AFM imaging (Figure S2a) and homogeneous PL [Figure 2a(E,F)]. We also measured C 1s, O 1s, N 1s, and S 2p X-ray photoelectron spectroscopy (XPS) spectra of the nondegraded and degraded film, to verify whether the exposure to light in an


DOI: 10.1021/acs.chemmater.9b02996
Chem. Mater. 2019, 31, 8927−8936

ambient atmosphere caused any substantial chemical modification of the film surface. No detectable changes in the film were observed upon degradation (Figure S3).

However, the PL spectra (Figure 3a) for the fresh (0 min) and degraded (10 min of degradation) sample are very different. Besides 6.7 times lower intensity, the spectrum red-shifted from 664 to 704 nm. The time evolution of the PL spectrum during degradation can be found in the Supporting Information (Figure S4). Contrary to the PL spectrum, the change in the absorption spectrum was small (Figure 3a). We point out, however, the visible suppression of the 0−0 absorption transition relative to 0−1 transition upon photodegradation.

We also found that the extent of polarization modulation of the fresh sample is somehow dependent on the substrate the film was prepared on. Figure S6 shows the situation for the film prepared on a silicon substrate. Substantial polarization was observed already in the fresh film while the PL spectrum was identical to the spectrum for the film on glass. After degradation the modulation increases, the spectrum red-shifted in the same way as on glass. Therefore, we conclude that qualitatively the same behavior was observed for the films on the silicon substrate besides a higher PL polarization degree.

## DISCUSSIONS

Our results show that the almost 10 times decrease of the PL intensity and the substantial change of the PL spectrum must be caused by a mechanism which is accompanied by only a very small change of the absorption spectrum and practically undetectable changes of morphology and chemical composition as revealed by AFM and PL imaging and XPS. A feasible mechanism is a formation of PL quenching sites at very low concentration, which, however, is able to quench almost all the PL because of an efficient exciton diffusion (energy transfer) over tens of nanometers in CPs.[47,48]

The homogeneous film morphology also indicates that the pattern in the $M_{em}$ image and the emission phase image [Figure 2a(C,E,F)] do not come from the large morphological defects of the film forming during spin-casting. These structures must be microscale-oriented domains in the otherwise very smooth film that are visible only in polarization microscopy. These domains are somehow hidden in the fresh sample on glass [Figure 2a(A)] but show up clearly [Figure 2a(B)] after the PL yield is decreased by photodegradation.

How can we explain the better visibility of the oriented domains in $M_{em}$ images in degraded samples? We can see two possibilities: (i) the oriented polymer domains become somehow more oriented (emit more polarized light) in spite of lower PL yield because of degradation or (ii) contribution of the PL of highly oriented domains to the total PL increases upon degradation of the film. In the latter case the PL of the less oriented phase should be quenched more than that of the more oriented phase upon photodegradation and by this the most oriented phase becomes more visible. We do not see any obvious mechanism for the first situation. Also it seems to contradict the strong change in the shape of the PL spectrum upon degradation. The second situation, however, is feasible as will be shown below. Therefore, we propose that the polymer film locally is a mixture of two phases which we call Phase 1 (less oriented, less photostable) and Phase 2 (more oriented, more photostable). Both phases possess some degree of anisotropy characterized by modulation depth $M_1$ and $M_2$ ($M_2 > M_1$) and the same orientation direction.

First of all, let us see if the two-phase model can account for the observed experimental data. Let us assume that the more oriented Phase 2 possesses a red-shifted PL spectrum with the maximum around 700 nm in comparison with the less oriented Phase 1 whose PL spectrum is peaking at 670 nm. Then if the PL of Phase 2 is more stable than the PL of Phase 1, after degradation we will see mostly phase 2 reproducing the red shift of the spectrum.

Assuming that the total emission intensity is the sum of the emission intensities of Phase 1 ($PL_1$) and phase 2 ($PL_2$), respectively, let us find possible combinations of modulation depths ($M_1$, $M_2$) and the contributions of the both phases ($\beta_1$, $\beta_2$) to the PL which do not contradict to the experimental data. These combinations should fit the substantial PL spectra change and the increasing of the overall modulation depth ($M_{em}$) upon photodegradation. From the considerations shown below, we will see that such combinations ($M_1$, $M_2$, $\beta_1$, and $\beta_2$) can be found.

We derived in Section S6 of the Supporting Information the equation which allows calculating the modulation depth ($M_{em}$) of a film consisted of two phases

$$M_{em} = \beta_1 M_1 + \beta_2 M_2 \tag{1}$$

where $M_1$ and $M_2$ are the modulation depths of Phase 1 and Phase 2, and $\beta_1$ and $\beta_2$ are the contributions of each phase to the total PL defined as

$$\beta_1 = \frac{PL_1}{PL_1 + PL_2} \tag{2}$$

$$\beta_2 = \frac{PL_2}{PL_1 + PL_2} \tag{3}$$

$$\beta_1 + \beta_2 = 1 \tag{4}$$

Using eq 4, we can rewrite eq 1 and show that $M_{em}$ is linearly dependent on the PL relative contribution $\beta_2$ from Phase 2

$$M_{em} = (M_2 - M_1)\beta_2 + M_1 \tag{5}$$

We would like to use this equation to determine the modulation depth $M_1$ and $M_2$ of the pure phases. For that we need to know the total modulation depth $M_{em}$ and $\beta_2$ for the initial and degraded sample. For the film on glass we know $M_{em}$ from 2D POLIM (0.07 initially and 0.14 after degradation). To estimate the relative contributions of each phase to the total PL we measured the time evolution of the PL intensity for the film on glass and successfully fitted it with a double exponential decay (Figure 4b). Assuming that the PL of each phase degrades exponentially over time, we assign the fast exponent to $PL_1$ and the slow one to $PL_2$. This fit allows us to estimate $\beta_1$(initial) = 0.71, $\beta_2$(initial) = 0.29 and after degradation $\beta_1$(final) = 0, $\beta_2$(final) = 1. Thus, we obtain coordinates of the two points shown by red dots in Figure 4a. The line passing through these points is then the linear function according to eq 5. The intercepts of the line with the vertical axes give us the modulation depths of the pure phases $M_1 = M_{em}(0) = 0.05$ and $M_2 = M_{em}(1) = 0.14$ for the film on glass.

For the film on the silicon substrate (Figure 4a, Silicon) we measured only the initial and final PL intensity. That is why we cannot apply the analysis of the time-dependent PL presented in Figure 4b. However, based on all the available experimental data, we are still able to define quite narrow limits for the possible values of $\beta_2$, namely, $0.125 < \beta_2(\text{initial}) < 0.65$ and



DOI: 10.1021/acs.chemmater.9b02996
Chem. Mater. 2019, 31, 8927−8936

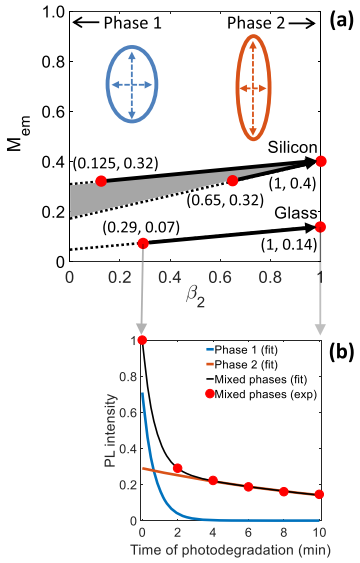


**Figure 4.** (a) Modulation depth in emission $M_{em}(\beta_2)$ where $\beta_2$ is the relative contribution of Phase 2 to the total PL, shown for the film on glass and silicon substrates. $M_{em}(0) = M_1$ is the modulation depth of pure Phase 1 (blue ellipse) and $M_{em}(1) = M_2$ is the modulation depth of pure Phase 2 (orange ellipse). The red points for the film on glass show the experimentally determined coordinates $(M, \beta_2)$ $(\beta_2, M)$ from 2D POLIM measurements $(M)$ and from the fitting of the PL intensity degradation kinetics shown in (b), see text for details. For the film on silicon we give the range of possible linear dependences depicted by the filled triangle.

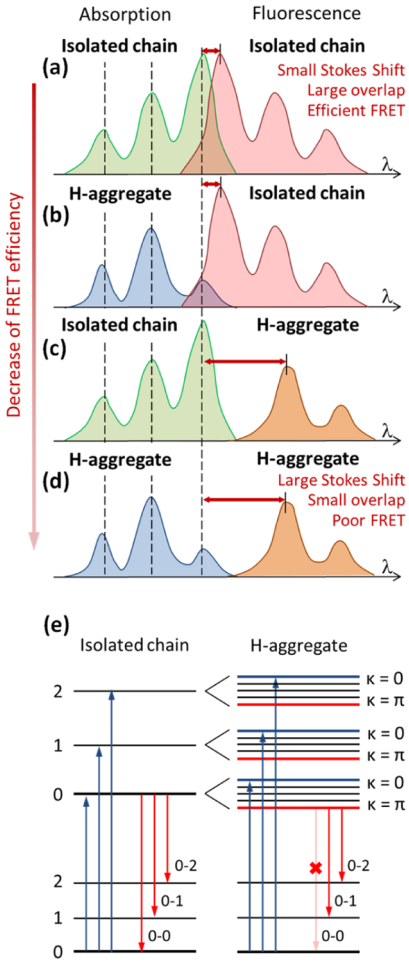


**Figure 5.** Because of the increase of Stokes shift, FRET efficiency of the donor–acceptor pairs decreases from (a–d). Cartoons showing absorption and PL spectra of (a) isolated chains, (b) isolated chains and H-aggregates, (c) H-aggregates and isolated chains, (d) H-aggregates. The species whose PL spectrum is shown works as an energy donor for the species whose absorption spectrum is shown (an energy acceptor). (e) Simplified energy level diagrams of an isolated chromophore (left) and an ideal H-aggregate with weak coupling (right), 0, 1, and 2 are vibrational levels of the ground (bottom) and excited (top) electronic state. In the diagram for the H-aggregate, blue levels are $k = 0$ excitons, and red levels are $k = \pi$ excitons. 0–0 transition in the emission of the H-aggregate is entirely absent because of the selection rules, while the other vibronic transitions are allowed.[50]

$\beta_2(\text{final}) \approx 1$, see the Supporting Information for details. Therefore, for the film on the silicon substrate, $M_1$ should be between 0.17 and 0.3, and $M_2 \approx 0.4$ as shown in Figure 4a (silicon). (More details in Section S7, Supporting Information)

From the 2D POLIM images and calculated $M_1$ and $M_2$ we see that the polymer chains have better alignment on the silicon compared to the glass substrate. Most probably this is because the surface energy of silicon is lower than that of glass. Indeed, it has been demonstrated that films coated on the lower surface energy substrate have longer time for chain reorientation in solution flow resulting in a higher degree of crystallinity and alignment.[49]

Now, when we have shown that the two-phase model is feasible, let us go back to the question why Phase 1 (less oriented phase having a normal PL spectrum) degrades much faster than Phase 2 (red-shifted PL spectrum). What is the physical mechanism behind that? Here we have reached the point where the nature of the polymer aggregates and the Förster resonance energy transfer (FRET) in the film (Figure 2d) needs to be discussed.

For the highly oriented phase (Phase 2) possessing distinctly polarized PL, neighboring polymer chains must be aligned in a parallel fashion as illustrated in Figure 6. Parallel arrangement of the chains creates favorable conditions for interaction between them (dipole–dipole long range interaction, or $\pi$–$\pi$ stacking at a shorter range) resulting in the formation of collective Frenkel excitons (H-/J-aggregates)[50] or even interchain species (excimers, exciplexes, and charge transfer excitons).[51] Compared to the loosely packed individual chains, such aggregates possess red-shifted PL spectra, which fits with the red-shifted PL spectra observed experimentally for Phase 2 in our films.

The optical and electronic properties of CP films are highly related to the energy transfer,[52−54] which can be assessed by fluorescence anisotropy[55,56] (in isotropically absorbing samples) and by the energy funnelling parameter[42−44] in oriented samples like those studied here. In general, EET by the Förster mechanism depends on the overlap between the emission spectrum of the energy donor and the absorption spectrum of the energy acceptor.[57] For homo FRET (FRET between similar chromophores), the larger the Stokes shift, the smaller is the FRET efficiency expected. Our experimental data is not enough to unambiguously tell the type of aggregates Phase 2 contains because both the interchain species (excimer, exciplexes, and charge transfer excitons) and Frenkel excitons formed in weakly coupled H- or J-aggregates are expected to show red-shifted PL spectra.



DOI: 10.1021/acs.chemmater.9b02996
Chem. Mater. 2019, 31, 8927–8936

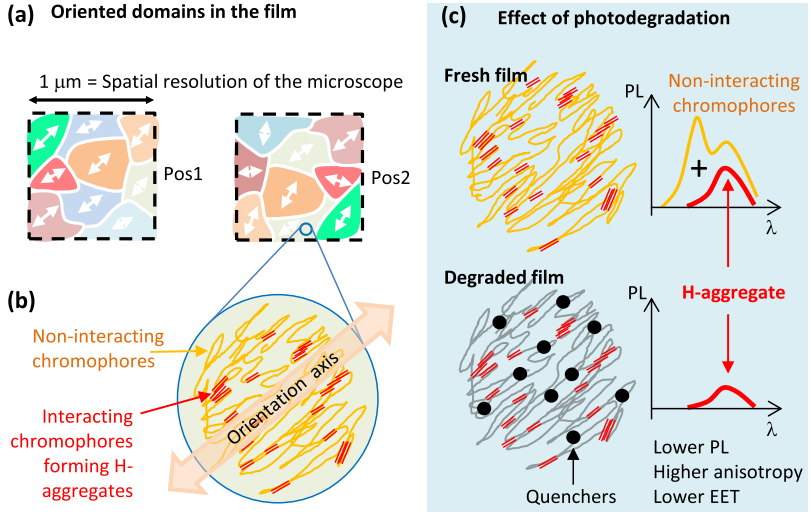


**Figure 6.** (a) Proposed local organization of the film which gives polarized PL (Pos1, high $M_{em}$) and unpolarized PL (Pos2, low $M_{em}$) when observed with our spatial resolution. These cartoons illustrate the domain organization in Pos1 and Pos2 marked in Figure 2b. (b) Proposed microscopic organization of one domain. Yellow long lines show polymer chains which do not have strong interaction between chain segments, but, still follow the predominant global orientation axis (Phase 1). Excitons are localized on individual segments in this phase, and energy transfer is very efficient between the individual segments there (Figure 5a). The red double lines show parallel segments having substantial excitonic interaction forming H-aggregates. The exciton states H-aggregates are weakly coupled excited states of the individual segments. The emission of H-aggregate is red-shifted (Figure 5e). (c) PL spectra of fresh and photodegraded films. PL of the fresh film is the sum of the PL of individual segments (Phase 1) and the PL of H-aggregates (Phase 2). The degraded film emits red-shifted PL (emission of H-aggregates) because the PL of individual segments is quenched because of efficient FRET to the photogenerated quenchers (black dots) formed in the nonaggregated phase.

Note that the emission of interchain species is not always easy to detect because of low transition dipole moment.[51] However, in our case, we still see a quite strong emission of Phase 2 (more oriented phase), and the PL lifetime of Phase 1 (less oriented phase) and Phase 2 are quite similar (Figure 3b). In addition, interchain species are expected to have a lower polarization degree.[58] Thus, interchain species are not likely what we observed. However, formation of weakly coupled H-aggregates looks feasible as will be discussed below.

The collective Frenkel excitons can be classified into J- and H- type depending on whether the transition dipole moments of the aggregated molecules are oriented in the head-to-tail fashion (J-aggregation) or parallel fashion (H-aggregation).[59] Parallel chain orientation in closed-packed regions creates ideal conditions for the formation of H-aggregates in CPs.[8,50] For an ideal weakly coupled H-aggregate ($V \ll$ vibronic frequency), 0−0 in the absorption peak is attenuated relative to the 0−1 peak because of interband mixing between the bands with various numbers of vibrational quanta[60] while in luminescence 0−0 transition becomes totally forbidden because of symmetry reasons (Figure 5e), and therefore, 0−1 transition appears as the strongest band in the spectra, comparing Figure 5a,c. In reality, the disorder makes 0−0 transition still possible and the effect of weak H-aggregation appears as a redistribution of the transition strength between the vibronic levels in comparison to that of the monomer (isolated chain). Thus, the suppression of 0−0 transition in the absorption spectra together with the red shift of the PL spectrum are strong indicators that the oriented domains in Phase 2 are weakly coupled H-aggregates.

Moreover, redistribution of the oscillator strength between the vibronic bands in a weakly coupled H-aggregate can explain why the energy transfer is poor in Phase 2. Let us consider FRET efficiency for the film containing Phase 1 (loosely packed individual chains) and Phase 2 (H-aggregates). Different situations are shown in Figure 5a−d. If we judge the FRET efficiency only by the spectral overlap between the emission of the donor and absorption of the acceptor, the highest efficiency of EET is expected for the case of FRET between individual chains. Because of much larger Stokes shift, EET from individual chains to aggregates should be smaller, while EET from aggregates to aggregates is probably not possible at all in the framework of the classical FRET mechanism. Therefore, the energy transfer efficiency within Phase 1 (loosely packed individual chains) must be much larger than that within Phase 2 (H-aggregates).

Photodegradation destroys and converts the emitting sites to luminescence quenchers leading to the suppression of the overall PL intensity. Because of efficient energy transfer within Phase 1, one quencher can quench a large volume of the film (hundreds of cubic nanometers). Therefore, the suppression of the emission of Phase 1 is very strong (Figure 6c). Because the energy transfer in CPs occurs at a time scale of picoseconds,[47] we are not able to see any changes in the PL decay upon quenching (Figure 3) due to limited time resolution and the process appears as static quenching.[61] However, if a quencher is formed in Phase 2 (H-aggregates) it does not influence substantially the PL of other aggregates and Phase 1 because they do not "feel" its presence because of the poor mutual energy transfer. Thus, the PL of Phase 2-containing aggregates is much less sensitive to the photodegradation in comparison with the Phase 1-containing loosely packed individual chains. This explains how photodegradation makes visible the aggregates which initially are hardly visible in the freshly prepared spin-cast film (Figure 6c).

The discussion above allows us to propose the view on the polymer organization and energy transfer in the film as schematically illustrated in Figure 6. The semicrystalline CP PBDT-TPD has a predominant global orientation at the micrometer scale (Figure 6a). Within these oriented "molds"/domains, there are large amounts of individual segments



DOI: 10.1021/acs.chemmater.9b02996
Chem. Mater. 2019, 31, 8927−8936

(Figure 6b, yellow long lines) possessing blue PL spectra (normal spectra), and a small amount of H-aggregates (Figure 6b, red short lines) possessing red-shifted PL spectra. Photodegradation of the polymer film first of all affects the material where the excitations spend most of the time, that is, in the low-energy emitting sites where the excitations are collected because of energy transfer. The emitting sites are mostly located among isolated individual segments because of poor energy transfer to H-aggregates. Thus, photodegradation generates more luminescence quenchers (Figure 6c, black dots) within the area of individual segments rather than in H-aggregates and also the efficiency of one quencher in the dominant phase of the individual segments is higher because of more efficient energy transfer. Consequently, the suppression of the PL intensity of individual segments is much stronger than for H-aggregates, which makes H-aggregates more visible in the degraded film.

Let us come back to the observed inhomogeneity of the polarization contrasts of the degraded film. In order to explain why different areas possess a different increase of $M_{em}$ (Figure 2) we need to realize that initially $M_{em}$ is low not only because of dominant contribution of Phase 1, but also due to the ensemble averaging over the spatial resolution of the microscope. In the degraded film, a region can possess high $M_{em}$ only if most of the original oriented "molds"/domains had a similar global orientation (see Pos1, Figure 6a). On the contrary, regions consisting of small oriented domains with different orientations possess lower $M_{em}$ due to the spatial averaging (see Pos2, Figure 6a). Then removing of the weakly oriented Phase 1 does not help to get high polarization in regions like Pos2 because of ensemble averaging. Note that such structures one can see only in the $M_{em}$ image [Figure 2a(B)] but not in the PL intensity image (Figure S5).

We did two more preliminary experimental tests (Sections S8 and S9, Supporting Information) which in general agree with our view on the polymer film illustrated in Figure 6 and also show possible further directions of this study. We found that thermal annealing neither changes the visible polarization structure of the film, nor its PL spectrum. This is because the film contains a high concentration of tightly aggregated chains which cannot be simply melted by elevating the temperature. However, solvent vapor annealing (SVA) over a long time changed the morphology dramatically. Given time, the polymer chains under SVA become more oriented forming very large oriented domains. SVA treatment results in more H-aggregates formed and to the red-shifted PL spectrum of the whole film even without any degradation imposed.

## CONCLUSIONS

We demonstrated that partial photodegradation of CP films can help reveal the internal organization of the material on the micro and macro levels. It tuned out that depending on the local peculiarities of electronic and vibrational transitions and energy transfer, the resistance of the polymer luminescence to photodegradation-induced quenching can be very different. It gave us a tool for visualization of hidden morphological structures of H-aggregate character by polarization luminescence microscopy. We found that the long-range order in terms of a predominant chain orientation can occur even on the micrometer scale in polymer films, which are usually considered isotropic. This diversity of structural organization in nominally uniform materials are expected to affect charge transport and charge photogeneration which is relevant for understanding and improving of polymer-based organic photovoltaic devices.

## ASSOCIATED CONTENT

### Supporting Information

The Supporting Information is available free of charge on the ACS Publications website at DOI: 10.1021/acs.chemmater.9b02996.

2D polarization portrait and the definition of the polarization parameters; AFM images and XPS spectra of nondegraded and degraded PBDT-TPD films; evolution of PL spectra and normalized images of the PBDT-TPD film on the glass substrate upon photodegradation (additional information for Figures 2 and 3); PL spectra and 2D POLIM images of the PBDT-TPD film on the silicon substrate; two-phase model of the polymer film composition; estimation of $\beta_2$ in the fresh film on silicon substrates; thermal annealing of the PBDT-TPD film on the glass substrate; and SVA of the PBDT-TPD film on the glass substrate (PDF)

## AUTHOR INFORMATION


### Corresponding Author

*E-mail: ivan.scheblykin@chemphys.lu.se.

### ORCID

Juanzi Shi: 0000-0002-9820-4460
Xiaofeng Xu: 0000-0002-4501-9579
Yuxin Xia: 0000-0002-2566-5645
Ruiyun Chen: 0000-0002-0037-856X
Zafer Hawash: 0000-0001-9606-3521
Ellen Moons: 0000-0002-1609-8909
Olle Inganäs: 0000-0002-6243-1450
Ivan G. Scheblykin: 0000-0001-6059-4777


### Notes

The authors declare no competing financial interest.

## ACKNOWLEDGMENTS

The work was supported by the Swedish Research Council, project 2016-04433, the Knut and Alice Wallenberg foundation project nos: 2016.0059, and through a Wallenberg Scholar grant to O.I. J.S., and Y.X. thank the China Scholarship Council (grants CSC nos: 201608110147 and 201406780008) for Ph.D scholarships. We thank the beamline staff at the SOLARIS national synchrotron facility in Krakow, Poland, for technical assistance.

## REFERENCES


(1) Sirringhaus, H. 25th Anniversary Article: Organic Field-Effect Transistors: The Path beyond Amorphous Silicon. *Adv. Mater.* **2014**, *26*, 1319−1335.

(2) Lee, S. Y.; Yasuda, T.; Komiyama, H.; Lee, J.; Adachi, C. Thermally Activated Delayed Fluorescence Polymers for Efficient Solution-Processed Organic Light-Emitting Diodes. *Adv. Mater.* **2016**, *28*, 4019−4024.

(3) Hou, J.; Inganäs, O.; Friend, R. H.; Gao, F. Organic Solar Cells Based on Non-Fullerene Acceptors. *Nat. Mater.* **2018**, *17*, 119−128.

(4) Rivnay, J.; Inal, S.; Salleo, A.; Owens, R. M.; Berggren, M.; Malliaras, G. G. Organic Electrochemical Transistors. *Nat. Rev. Mater.* **2018**, *3*, 17086.

(5) Zeglio, E.; Inganäs, O. Active Materials for Organic Electrochemical Transistors. *Adv. Mater.* **2018**, *30*, 1800941.




DOI: 10.1021/acs.chemmater.9b02996
*Chem. Mater.* 2019, 31, 8927−8936

(6) Inal, S.; Rivnay, J.; Suiu, A.-O.; Malliaras, G. G.; McCulloch, I. Conjugated Polymers in Bioelectronics. *Acc. Chem. Res.* **2018**, *51*, 1368−1376.
(7) Van De Burgt, Y.; Melianas, A.; Keene, S. T.; Malliaras, G.; Salleo, A. Organic Electronics for Neuromorphic Computing. *Nat. Electron.* **2018**, *1*, 386−397.
(8) Hestand, N. J.; Spano, F. C. Expanded Theory of H- and J-Molecular Aggregates: The Effects of Vibronic Coupling and Intermolecular Charge Transfer. *Chem. Rev.* **2018**, *118*, 7069−7163.
(9) Baghgar, M.; Labastide, J.; Bokel, F.; Dujovne, I.; McKenna, A.; Barnes, A. M.; Pentzer, E.; Emrick, T.; Hayward, R.; Barnes, M. D. Probing Inter- and Intrachain Exciton Coupling in Isolated Poly(3-Hexylthiophene) Nanofibers: Effect of Solvation and Regioregularity. *J. Phys. Chem. Lett.* **2012**, *3*, 1674−1679.
(10) Yamagata, H.; Hestand, N. J.; Spano, F. C.; Köhler, A.; Scharsich, C.; Hoffmann, S. T.; Bässler, H. The Red-Phase of Poly[2-Methoxy-5-(2-Ethylhexyloxy)- 1,4-Phenylenevinylene] (MEH-PPV): A Disordered HJ-Aggregate. *J. Chem. Phys.* **2013**, *139*, 114903.
(11) Samuelsen, E. J.; Monkman, A. P.; Pettersson, L. A. A.; Horsburgh, L. E.; Aasmundtveit, K. E.; Ferrer, S. The Structure of Polypyridine. *Synth. Met.* **2001**, *124*, 393−398.
(12) Pettersson, L. A. A.; Ghosh, S.; Inganäs, O. Optical Anisotropy in Thin Films of Poly(3,4-Ethylenedioxythiophene)- Poly(4-Styrenesulfonate). *Org. Electron.* **2002**, *3*, 143−148.
(13) Persson, N.; Schubert, M.; Inganäs, O. Optical Modelling of a Layered Photovoltaic Device with a Polyfluorene Derivative/Fullerene as the Active Layer. *Sol. Energy Mater. Sol. Cells* **2004**, *83*, 169−186.
(14) Persson, N.-K.; Arwin, H.; Inganas, O. Optical Optimization of Polyfluorene-Fullerene Blend Photodiodes. *J. Appl. Phys.* **2005**, *97*, 034503.
(15) Zhokhavets, U.; Erb, T.; Hoppe, H.; Gobsch, G.; Serdar Sariciftci, N. Effect of Annealing of Poly(3-Hexylthiophene)/Fullerene Bulk Heterojunction Composites on Structural and Optical Properties. *Thin Solid Films* **2006**, *496*, 679−682.
(16) Chuang, S.-Y.; Chen, H.-L.; Lee, W.-H.; Huang, Y.-C.; Su, W.-F.; Jen, W.-M.; Chen, C.-W. Regioregularity Effects in the Chain Orientation and Optical Anisotropy of Composite Polymer/Fullerene Films for High-Efficiency, Large-Area Organic Solar Cells. *J. Mater. Chem.* **2009**, *19*, 5554−5560.
(17) Bergqvist, J.; Arwin, H.; Inganäs, O. Uniaxial Anisotropy in PEDOT:PSS Electrodes Enhances the Photocurrent at Oblique Incidence in Organic Solar Cells. *ACS Photonics* **2018**, *5*, 3023−3030.
(18) Yang, H.; Shin, T. J.; Bao, Z.; Ryu, C. Y. Structural Transitions of Nanocrystalline Domains in Regioregular Poly(3-Hexyl Thiophene) Thin Films. *J. Polym. Sci. B Polym. Phys.* **2007**, *45*, 1390−1398.
(19) Grell, M.; Bradley, D. D. C.; Ungar, G.; Hill, J.; Whitehead, K. S. Interplay of Physical Structure and Photophysics for a Liquid Crystalline Polyfluorene. *Macromolecules* **1999**, *32*, 5810−5817.
(20) Lee, L. F.; Adronov, A.; Schaller, R. D.; Fréchet, J. M. J.; Saykally, R. J. Intermolecular Coupling in Nanometric Domains of Light-Harvesting Dendrimer Films Studied by Photoluminescence near-Field Scanning Optical Microscopy (PL NSOM). *J. Am. Chem. Soc.* **2003**, *125*, 536−540.
(21) Adachi, T.; Brazard, J.; Chokshi, P.; Bolinger, J. C.; Ganesan, V.; Barbara, P. F. Highly Ordered Single Conjugated Polymer Chain Rod Morphologies. *J. Phys. Chem. C* **2010**, *114*, 20896−20902.
(22) Lin, H.; Tabaei, S. R.; Thomsson, D.; Mirzov, O.; Larsson, P.-O.; Scheblykin, I. G. Fluorescence Blinking, Exciton Dynamics, and Energy Transfer Domains in Single Conjugated Polymer Chains. *J. Am. Chem. Soc.* **2008**, *130*, 7042−7051.
(23) Watts, B.; Schuettfort, T.; McNeill, C. R. Mapping of Domain Orientation and Molecular Order in Polycrystalline Semiconducting Polymer Films with Soft X-Ray Microscopy. *Adv. Funct. Mater.* **2011**, *21*, 1122−1131.
(24) Schuettfort, T.; Watts, B.; Thomsen, L.; Lee, M.; Sirringhaus, H.; McNeill, C. R. Microstructure of Polycrystalline PBTTT Films: Domain Mapping and Structure Formation. *ACS Nano* **2012**, *6*, 1849−1864.
(25) Martino, N.; Fazzi, D.; Sciascia, C.; Luzio, A.; Antognazza, M. R.; Caironi, M. Mapping Orientational Order of Charge-Probed Domains in a Semiconducting Polymer. *ACS Nano* **2014**, *8*, 5968−5978.
(26) Takacs, C. J.; Treat, N. D.; Krämer, S.; Chen, Z.; Facchetti, A.; Chabinyc, M. L.; Heeger, A. J. Remarkable Order of a High-Performance Polymer. *Nano Lett.* **2013**, *13*, 2522−2527.
(27) Kuehn, S.; Pingel, P.; Breusing, M.; Fischer, T.; Stumpe, J.; Neher, D.; Elsaesser, T. High-Resolution near-Field Optical Investigation of Crystalline Domains in Oligomeric PQT-12 Thin Films. *Adv. Funct. Mater.* **2011**, *21*, 860−868.
(28) Täuber, D.; Cai, W.; Inganäs, O.; Scheblykin, I. G. Macroscopic Domains within an Oriented TQ1 Film Visualized Using 2D Polarization Imaging. *ACS Omega* **2017**, *2*, 32−40.
(29) Vohra, V.; Arrighetti, G.; Barba, L.; Higashimine, K.; Porzio, W.; Murata, H. Enhanced Vertical Concentration Gradient in Rubbed P3HT:PCBM Graded Bilayer Solar Cells. *J. Phys. Chem. Lett.* **2012**, *3*, 1820−1823.
(30) Anzai, T.; Porzio, W.; Vohra, V. Polarized Emission from Conjugated Polymer Chains Aligned by Epitaxial Growth during Off-Center Spin-Coating. *J. Chem.* **2017**, *2017*, 1−9.
(31) Baliyan, V. K.; Kumar, V.; Kim, J.; Kang, S.-W. Polarized Photoluminescence of the Polymer Networks Obtained by in Situ Photopolymerization of Fluorescent Monomer in a Nematic Liquid Crystal. *Opt. Mater. Express* **2016**, *6*, 2956.
(32) Xu, X.; Li, Z.; Zhang, W.; Meng, X.; Zou, X.; Di Carlo Rasi, D.; Ma, W.; Yartsev, A.; Andersson, M. R.; Janssen, R. A. J.; et al. 8.0% Efficient All-Polymer Solar Cells with High Photovoltage of 1.1 V and Internal Quantum Efficiency near Unity. *Adv. Energy Mater.* **2018**, *8*, 1700908.
(33) Li, G.; Chang, W. H.; Yang, Y. Low-Bandgap Conjugated Polymers Enabling Solution-Processable Tandem Solar Cells. *Nat. Rev. Mater.* **2017**, *2*, 17043.
(34) Zhang, G.; Fu, Y.; Qiu, L.; Xie, Z. Synthesis and Characterization of Thieno[3,4-c]Pyrrole-4,6-Dione and Pyrrolo[3,4-c]Pyrrole-1,4-Dione-Based Random Polymers for Photovoltaic Applications. *Polymer* **2012**, *53*, 4407−4412.
(35) He, M.; Wang, M.; Lin, C.; Lin, Z. Optimization of Molecular Organization and Nanoscale Morphology for High Performance Low Bandgap Polymer Solar Cells. *Nanoscale* **2014**, *6*, 3984−3994.
(36) Zhao, W.; Ye, L.; Zhang, S.; Sun, M.; Hou, J. A Universal Halogen-Free Solvent System for Highly Efficient Polymer Solar Cells. *J. Mater. Chem. A* **2015**, *3*, 12723−12729.
(37) Yuan, J.; Zhai, Z.; Dong, H.; Li, J.; Jiang, Z.; Li, Y.; Ma, W. Efficient Polymer Solar Cells with a High Open Circuit Voltage of 1 Volt. *Adv. Funct. Mater.* **2013**, *23*, 885−892.
(38) Kim, J.-H.; Park, J. B.; Xu, F.; Kim, D.; Kwak, J.; Grimsdale, A. C.; Hwang, D.-H. Effect of $\pi$-Conjugated Bridges of TPD-Based Medium Bandgap Conjugated Copolymers for Efficient Tandem Organic Photovoltaic Cells. *Energy Environ. Sci.* **2014**, *7*, 4118−4131.
(39) Tubasum, S.; Scheblykin, I. G.; Yadav, D.; Pullerits, T.; Cogdell, R. J.; Camacho, R.; Meyer, M. Evidence of Excited State Localization and Static Disorder in LH2 Investigated by 2D-Polarization Single-Molecule Imaging at Room Temperature. *Phys. Chem. Chem. Phys.* **2013**, *15*, 19862−19869.
(40) Camacho, R.; Thomsson, D.; Sforazzini, G.; Anderson, H. L.; Scheblykin, I. G. Inhomogeneous Quenching as a Limit of the Correlation between Fluorescence Polarization and Conformation of Single Molecules. *J. Phys. Chem. Lett.* **2013**, *4*, 1053−1058.
(41) Thomsson, D.; Camacho, R.; Tian, Y.; Yadav, D.; Sforazzini, G.; Anderson, H. L.; Scheblykin, I. G. Cyclodextrin Insulation Prevents Static Quenching of Conjugated Polymer Fluorescence at the Single Molecule Level. *Small* **2013**, *9*, 2619−2627.
(42) Camacho, R.; Täuber, D.; Scheblykin, I. G. Fluorescence Anisotropy Reloaded—Emerging Polarization Microscopy Methods for Assessing Chromophores' Organization and Excitation Energy Transfer in Single Molecules, Particles, Films, and Beyond. *Adv. Mater.* **2019**, *31*, 1805671.


DOI: 10.1021/acs.chemmater.9b02996
*Chem. Mater.* 2019, 31, 8927−8936

(43) Camacho, R.; Thomsson, D.; Yadav, D.; Scheblykin, I. G. Quantitative Characterization of Light-Harvesting Efficiency in Single Molecules and Nanoparticles by 2D Polarization Microscopy: Experimental and Theoretical Challenges. *Chem. Phys.* **2012**, *406*, 30−40.
(44) Camacho, R.; Täuber, D.; Hansen, C.; Shi, J.; Bousset, L.; Melki, R.; Li, J.-Y.; Scheblykin, I. G. 2D Polarization Imaging as a Low-Cost Fluorescence Method to Detect α-Synuclein Aggregation Ex Vivo in Models of Parkinson's Disease. *Commun. Biol.* **2018**, *1*, 157.
(45) Tian, Y.; Scheblykin, I. G. Artifacts in Absorption Measurements of Organometal Halide Perovskite Materials: What Are the Real Spectra? *J. Phys. Chem. Lett.* **2015**, *6*, 3466−3470.
(46) Alem, S.; Wakim, S.; Lu, J.; Robertson, G.; Ding, J.; Tao, Y. Degradation Mechanism of Benzodithiophene-Based Conjugated Polymers When Exposed to Light in Air. *ACS Appl. Mater. Interfaces* **2012**, *4*, 2993−2998.
(47) Scheblykin, I. G.; Yartsev, A.; Pullerits, T.; Gulbinas, V.; Sundström, V. Excited State and Charge Photogeneration Dynamics in Conjugated Polymers. *J. Phys. Chem. B* **2007**, *111*, 6303−6321.
(48) Lin, J. D. A.; Mikhnenko, O. V.; Chen, J.; Masri, Z.; Ruseckas, A.; Mikhailovsky, A.; Raab, R. P.; Liu, J.; Blom, P. W. M.; Loi, M. A.; et al. Systematic Study of Exciton Diffusion Length in Organic Semiconductors by Six Experimental Methods. *Mater. Horiz.* **2014**, *1*, 280−285.
(49) Zhang, F.; Mohammadi, E.; Luo, X.; Strzalka, J.; Mei, J.; Diao, Y. Critical Role of Surface Energy in Guiding Crystallization of Solution-Coated Conjugated Polymer Thin Films. *Langmuir* **2018**, *34*, 1109−1122.
(50) Spano, F. C. The Spectral Signatures of Frenkel Polarons in H- and J-Aggregates. *Acc. Chem. Res.* **2010**, *43*, 429−439.
(51) Schwartz, B. J. Conjugated Polymers As Molecular Materials : How Chain Conformation and Film Morphology Influence Energy Transfer and Interchain Interactions. *Annu. Rev. Phys. Chem.* **2003**, *54*, 141−172.
(52) Lemmer, U.; Göbel, E. O.; Bässler, H.; Greiner, A.; Wada, Y.; Mahrt, R. F. Picosecond Hopping Relaxation in Conjugated Polymers. *Chem. Phys. Lett.* **1993**, *209*, 243−246.
(53) Brunner, K.; van Haare, J. A. E. H.; Langeveld-Voss, B. M. W.; Schoo, H. F. M.; Hofstraat, J. W.; van Dijken, A. Mechanistic Study of Excitation Energy Transfer in Dye-Doped PPV Polymers. *J. Phys. Chem. B* **2002**, *106*, 6834−6841.
(54) Mahrt, R. F.; Wegmann, G.; Bässler, H.; Hennig, R.; Pauck, T.; Siegner, U.; Kurz, H.; Hopmeier, M.; Scherf, U.; Lemmer, U.; et al. Dynamics of Optical Excitations in a Ladder-Type π-Conjugated Polymer Containing Aggregate States. *Phys. Rev. B: Condens. Matter Mater. Phys.* **1996**, *54*, 1759−1765.
(55) Miki, M. The Recovery of the Polymerizability of Lysdl-Labelled Actin by the Addition of Phalloidin Fluorescence Polarization and Resonance-Energy-Transfer Measurements. *Eur. J. Biochem.* **1987**, *164*, 229−235.
(56) Xu, Q.-H.; Bazan, G. C.; Wang, S.; Moses, D.; Heeger, A. J.; Korystov, D.; Mikhailovsky, A. The Fluorescence Resonance Energy Transfer (FRET) Gate: A Time-Resolved Study. *Proc. Natl. Acad. Sci. U.S.A.* **2005**, *102*, 530−535.
(57) Lakowicz, J. R. *Principles of Fluorescence Spectroscopy*, 3rd ed.; Springer US: New York, 2006; pp 445.
(58) Camacho, R.; Meyer, M.; Vandewal, K.; Tang, Z.; Inganäs, O.; Scheblykin, I. G. Polarization Imaging of Emissive Charge Transfer States in Polymer/Fullerene Blends. *Chem. Mater.* **2014**, *26*, 6695−6704.
(59) Kobayashi, T.; Du, J.; Kida, Y. Ultrafast Real-time Vibrational Dynamics In J-Aggregates. In *J-Aggregates*; Kobayashi, T., Ed.; World Scientific: Singapore, 2012; Vol *2*, p 2.
(60) Spano, F. C. Absorption in Regio-Regular Poly(3-Hexyl)-Thiophene Thin Films: Fermi Resonances, Interband Coupling and Disorder. *Chem. Phys.* **2006**, *325*, 22−35.
(61) Sahoo, D.; Sugiyasu, K.; Tian, Y.; Takeuchi, M.; Scheblykin, I. G. Effect of Conjugated Backbone Protection on Intrinsic and Light-Induced Fluorescence Quenching in Polythiophenes. *Chem. Mater.* **2014**, *26*, 4867−4875.


DOI: 10.1021/acs.chemmater.9b02996
*Chem. Mater.* 2019, 31, 8927−8936